Steering of magnetic domain walls by single ultrashort laser pulses

Yasser A. Shokr,[1,2] Oliver Sandig,[1] Mustafa Erkovan,[3,4] Bin Zhang,[1,*] Matthias Bernien,[1] Ahmet A. Ünal,[5,†] Florian Kronast,[5] Umut Parlak,[6,‡] Jan Vogel,[7] and Wolfgang Kuch[1,§]

[1]*Institut für Experimentalphysik, Freie Universität Berlin, Arnimallee 14, 14195 Berlin, Germany*

[2]*Faculty of Science, Department of Physics, Helwan University, 17119 Cairo, Egypt*

[3]*Sakarya University of Applied Sciences, Mechanical Engineering, 54187 Sakarya, Turkey*

[4]*INESC-Microsystems and Nanotechnologies (INESC-MN), 1000-029 Lisboa, Portugal*

[5]*Helmholtz-Zentrum Berlin für Materialien und Energie, Albert-Einstein-Straße 15, 12489 Berlin, Germany*

[6]*Gebze Technical University, Physics Department, 41400 Kocaeli, Turkey*

[7]*Université Grenoble Alpes, CNRS, Institut Néel, 38000 Grenoble, France*

(Received 13 April 2018; revised manuscript received 12 April 2019; published 3 June 2019)

We present a magnetic domain-imaging study by x-ray magnetic circular dichroism photoelectron emission microscopy on a $Co/Fe_{75}Gd_{25}$ bilayer under exposure to single focused ultrashort (100 fs) infrared laser pulses. Magnetic domain walls experience a force in the intensity gradient of the laser pulses away from the center of the pulse, which can be used to steer domain walls to move in a certain direction. Maximum domain-wall displacements after individual laser pulses close to 1 μm in zero external field are observed. Quantitative estimates show that electronic spin currents from the spin-dependent Seebeck effect are not strong enough to explain the effect, which we thus attribute to the torque exerted by magnons from the spin Seebeck effect that are reflected at the domain wall.

DOI: 10.1103/PhysRevB.99.214404

I. INTRODUCTION

Research on how to move magnetic domain walls in artificially engineered materials is experiencing a high level of interest due to potential applications in computing technology and data storage media [1–3]. Besides domain-wall motion by magnetic fields and electric currents, laser-induced manipulation of magnetization is considered particularly interesting with respect to speed and power consumption [4]. Deterministic switching of magnetization by circularly polarized laser light has been demonstrated in magnetic insulators [5], semiconductors [6], as well as in metallic ferrimagnetic alloys and multilayers [7–10]. This allows one to use ultrashort laser pulses for writing or processing magnetic information. As previously demonstrated by some of us, ultrashort laser pulses are also able to move magnetic domain walls, even if their duration is much shorter than the time the domain wall needs to travel [11]. A stochastic back-and-forth motion of domain walls over several hundreds of nanometers could be triggered by ultrashort laser pulses [11,12], which has been attributed to laser-pulse-induced depinning of domain walls and successive thermal domain-wall motion [11]. Series of circularly polarized laser pulses were found to move domain walls in the direction defined by the pulse helicity if the intensity was below the threshold for all-optical magnetization reversal [13,14], while the average domain-wall displacement per laser pulse was of the order of a few nm. Since the Gaussian profile of an incoming focused laser pulse leads to a thermal gradient in the sample, this could be used, in addition, to define the direction of this laser-induced domain-wall motion. In fact, a controlled steering of domain walls is desired for applications, rather than a stochastic motion.

The possibility of steering magnetic domain walls by thermal gradients has received a lot of attention recently [6,15–24]. Different mechanisms have been proposed that can move a domain wall in a thermal gradient. The free energy of domain walls decreases with increasing temperature because of entropy, leading to an entropic force on the wall that pushes it towards the hotter region [15,16]. Magnonic spin currents passing from hotter to colder regions exert a torque on a domain wall due to conservation of angular momentum [17], the sign of which depends on whether the magnons pass nearly undisturbed through the domain wall or whether they are reflected at the wall [16,18,19]. In the former case, the domain wall moves in the direction opposite to the magnon propagation direction, i.e., to the hotter side [16–18], while reflection of magnons at the domain wall pushes it to the colder side [16,18,19]. Electronic spin currents due to the spin-dependent Seebeck effect could also lead to a torque on the domain wall [25,26]. Finally, a thermally induced dipolar field has been identified theoretically as a further driving force acting on a domain wall in a thermal gradient [16].

A few experiments on domain walls in thermal gradients are found in the literature [6,14,20–22]. In all of them, the force on the domain wall was in the direction towards the

*Present address: Huawei, Shenzhen, People's Republic of China.

†Present address: Max-Born-Institut für nichtlineare Optik und Kurzzeitspektroskopie, Max-Born-Straße 2 A, 12489 Berlin, Germany.

‡Present address: Electronic Properties (PGI-6), Peter Grünberg Institut, Forschungszentrum Jülich, 52425 Jülich, Germany.

§Corresponding author: kuch@physik.fu-berlin.de

hotter side. However, depending on material parameters, in particular on the width of the domain wall compared to the wavelength of propagating magnons, domain-wall motion towards the colder region due to magnon recoil at the domain wall could, in principle, also occur [16,18,19,23,24].

We present a domain-imaging study on Co/FeGd bilayers by photoelectron emission microscopy (PEEM) with x-ray magnetic circular dichroism (XMCD) as the magnetic contrast mechanism [27,28]. We show evidence for a propagation of domain walls of close to a micron in the photon-flux-density gradient of single 100 fs laser pulses away from the center of the laser spot, i.e., towards the colder region on the sample. A quantitative estimate rules electronic-current-induced domain-wall motion by the spin-dependent Seebeck effect as unlikely, such that we interpret this result as a consequence of the recoil of magnons from the (magnonic) spin Seebeck effect at the domain wall.

II. EXPERIMENT

The sample with structure 0.8 nm Pt/1 nm Co/15 nm Fe_{75} Gd_{25}/1 nm Pt/Si(001) was prepared by magnetron sputter deposition from elemental targets in a 1.2×10^{-3} mbar Ar atmosphere. A naturally oxidized Si(001) wafer, cleaned by ethanol and methanol and heated to 823 K for 20 min after transfer into the vacuum system, served as the substrate. After reintroducing the sample to ultrahigh vacuum, it was heated to 400 K for 30 min. Magnetic domain images were obtained by XMCD-PEEM using the Elmitec PEEM-II instrument at the UE-49 SPEEM beam line of BESSY II. During the measurements, the sample was mounted on a sample holder that allows one to apply a magnetic field during the PEEM image acquisition by a microcoil [29]. To enhance the spatial resolution, energy filtering of the electrons with about 0.2 eV resolution was applied. The acceleration potential between sample and first objective lens of the PEEM was set to 10 keV. All experiments were performed at 50 K sample temperature. At this temperature, which is far below the compensation temperature of the ferrimagnet [30], the Gd magnetization dominates and is aligned with the external field direction. Magnetic domain images acquired at the absorption maximum of the Gd M_5 edge at a photon energy of 1182.6 eV, using the fifth harmonic of the helical undulator, showed the best signal-to-noise contrast and are presented in the following. The field of view was adjusted to 20 μm. The laterally resolved XMCD intensity, measured from low-energy electron yield, is presented as gray-scale-contrast images, either directly showing the local yield for one helicity or calculated as the XMCD asymmetry, i.e., the difference between images acquired with opposite helicity divided by their sum [28]. Comparison of XMCD-PEEM images acquired at the Gd M_5, Fe L_3, and Co L_3 edges shows that the Gd magnetization is oriented opposite to both the Fe and Co magnetization directions [30]. The sample exhibits magnetic domains much larger than the field of view of the PEEM of 20–50 μm and magnetization reversal proceeds by propagation of straight domain walls over long distances. By increasing the external magnetic field carefully until the image contrast in PEEM is seen to reverse and then moving the sample a bit, it is possible to have such a domain wall within the field of view.

Magnetic fields were applied to the sample by an electromagnet mounted inside the sample holder, underneath the sample. At the imaged surface position, the field from this electromagnet consisted of in- and out-of-plane components. The current through the coil was carefully adjusted to compensate any in-plane field from the remanence of the core of the electromagnet or stray magnetic fields from the magnetic lenses of the electron optics of the PEEM or surrounding equipment by observing the onset of field-induced domain-wall motion for both polarities of the current. The field values given here are referenced to this field as zero. This compensation amounted to about half of the coercive field of the sample at 50 K. *Ex situ* magneto-optical Kerr effect (MOKE) measurements performed after the PEEM experiments showed only in-plane magnetization of the sample at temperatures below 220 K [30]. The coercivity was about 2.5 mT at 100 K. This value was used to calibrate the in-plane component of the magnetic field applied in the PEEM sample holder. Since there is no other means to calibrate this spatially varying field, the field values reported for our PEEM measurements refer to the assumption that the coercivity does not change significantly between 100 and 50 K [31], and may thus include a certain systematic error.

The end station at UE49-SPEEM is equipped with a Femtolasers Scientific XL Ti:sapphire oscillator. X rays and laser light impinge on the sample from opposite sides under a grazing angle of 16° to the surface. The laser system produces pulses with repetition rate of 5 MHz and pulse width down to 60 fs at a central wavelength of 800 nm. In this experiment, the pulse width was adjusted to 100 fs and set to single shot by using a Femtolasers Pulsfinder. The laser spot was focused by an optical lens inside the vacuum chamber to a spot size of 11×37 μm^2 (at $1/e$ of the maximum intensity) on the sample. The flux density was adjusted to 25 mJ/cm^2 in the center of the spot on the sample by a combination of a $\lambda/2$ plate and a polarizer. This number for the flux density includes a systematic error of about 20% related to the uncertainty in the spot size. The position of the laser spot was imaged for lower laser fluences from the PEEM intensity caused by three-photon photoemission processes at hot spots of the sample surface. An example is shown in the Supplemental Material [30]. The laser pulses are linearly p polarized at the sample with a degree of polarization of more than 95%. X-ray PEEM images taken at the position of the footprint of the laser on the sample after a series of single laser pulses with the fluences used here did not show any laser-induced modifications.

III. RESULTS AND DISCUSSION

To observe laser-induced magnetic domain-wall motion, the external field has to be carefully adjusted to zero. Before doing so, two nearby domain walls have been created as the starting configuration by applying small quasistatic fields of varying polarity around the strength of the coercive field. Figure 1(a) shows an XMCD asymmetry image of this configuration. These domain walls are found to be stable up to several hours without external magnetic field or laser pulses. The sample was placed such that the laser spot was approximately in the middle between the two domain walls, as indicated by the red ellipse in Fig. 1(a). We refer to

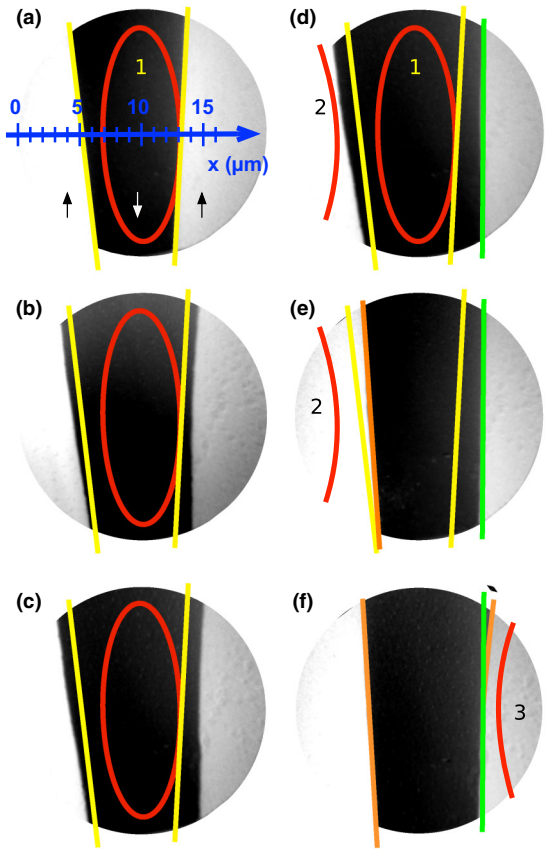

FIG. 1. Gd M_5 XMCD-PEEM asymmetry images taken at zero external magnetic field. (a) Starting configuration with two domain walls within the field of view. (b)–(d) After first, second, and third laser pulse, respectively, reaching the sample at the red ellipse labeled 1. (e) Domain image after nine pulses with the laser at the position marked by the ellipse labeled 2. (f) Domain image after nine pulses with the laser at position labeled 3. Yellow, green, and orange lines mark identical positions on the sample surface. The field of view is 20 μm. The blue axis in (a) is used to measure the position of the two domain walls; arrows indicate the local magnetization directions.

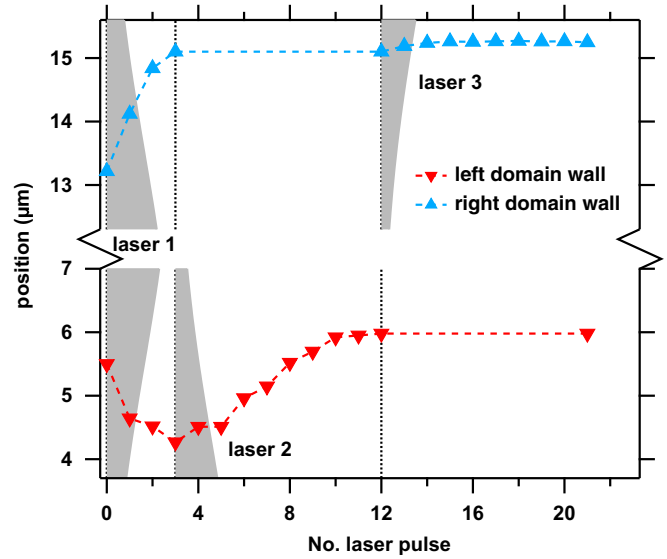

FIG. 2. Domain-wall positions of the two domain walls in Fig. 1 along the blue line shown in Fig. 1(a) as a function of the number of applied laser pulses at laser positions 1 (three pulses), 2 (nine pulses), and 3 (nine pulses). The respective laser positions are indicated by their gray-shaded Gaussian intensity profiles, plotted onto the vertical dashed lines as zero lines.

this position of the laser beam as "position 1." The image obtained after applying one laser pulse is shown in Fig. 1(b). Yellow, green, and orange lines mark identical positions in the different panels of Fig. 1. The effect of the laser pulse is to move both domain walls away from the center of the laser spot, i.e., to the colder regions of the sample. Figure 1(c) shows the effect of a second laser pulse, which further moved both domain walls apart from each other; Fig. 1(d) shows the sample after three laser pulses. A summary of this experiment is presented in Fig. 2. Here, the positions of the two domain walls along the blue line shown in Fig. 1(a) are plotted as a function of the number of applied laser pulses. During the three laser pulses applied at laser position 1, corresponding to a central position of 10.0 μm, both walls move apart from each other, with displacements becoming smaller from pulse to pulse. The laser profile is indicated by the gray-shaded plot of the Gaussian photon density of the laser spot, plotted as a function of the position as the vertical axis.

Next, the sample was placed in such a way that the laser was hitting left of the left domain wall, corresponding to a laser central position of 0.6 μm, indicated by the red ellipse labeled 2 in Figs. 1(d) and 1(e). Nine laser pulses were applied at that position and the position of the left domain wall was evaluated from XMCD-PEEM images acquired after each laser pulse. Figure 1(e) shows the result after moving the sample back to have the laser spot again at position 1. This can be done with very high precision of <50 nm by adjusting the image position with respect to small structural defects visible in the images. Note that in between, when imaging with the laser in position 2, the right domain wall is not within the field of view and hence its position cannot be determined. However, as seen from Fig. 1(e), it has not moved after these nine pulses. The position of the left domain wall is depicted in Fig. 2 (laser pulse 4–12). The wall moves back to the right, to higher-number positions, eventually exceeding the starting position. The position of the wall thereby exhibits a saturationlike behavior, with the displacement becoming smaller from pulse to pulse, while the domain wall moves away from the laser pulse, indicated by the gray-shaded profile labeled "laser 2." When the domain wall reaches a position of 5.9 μm, where the fluence is about 8 mJ/cm^2, the laser-induced domain-wall motion is nearly zero. Figure 1(e) shows the domain pattern after the ninth pulse.

Finally, the same experiment was repeated with the laser at position 3, centered at 19.5 μm, right of the right domain wall, indicated by the red ellipse in Fig. 1(f) and the respective gray-shaded profile in Fig. 2. In this situation, no clear directed domain-wall motion could be observed during the nine applied pulses. We attribute this to a strong pinning potential at that particular place of the sample, possibly by defects, trapping the right domain wall. Small changes of the

domain-wall position, with a certain back-and-forth character, are observed. The result after nine laser pulses is shown in Fig. 1(f). The difference between the orange and the green lines points out such a back-and-forth motion of the domain wall. More images are presented in the Supplemental Material [30]. It shows that the domain wall is depinned by the laser pulses in some sections, but held fixed at others, which hinders a directed motion of the domain wall. This can be explained by the presence of some relatively strong pinning sites at the position of this domain wall. Note that the domain walls always remained straight. No curving of the domain walls around the laser spot has been observed. We attribute this to the overall low density of pinning sites, such that minimization of the domain-wall energy leads to rather straight domain walls. On the other hand, this also means that one pinning site can block a large section of the domain wall.

These experiments show that domain walls can be steered back and forth just by laser pulses, provided that domain-wall pinning is sufficiently small. To estimate the strength of this effect, an external magnetic field of 1.1 mT, about 45% of the coercive field, has been applied. Laser-induced domain-wall motion is then observed after individual laser pulses, similar to the result presented in Ref. [11], while the direction of domain-wall motion is defined by the direction of the external magnetic field. Figure 3 summarizes the results of this experiment. Two PEEM images for positive helicity are shown as insets. A domain wall separates a domain with dark contrast on the left side from a domain with brighter contrast on the right side. Note that these are not asymmetry images like the ones shown in Fig. 1, but simply PEEM images acquired with one sense (positive) of circular helicity. The sample, and thus the domain wall, was positioned in such a way that the center of the laser spot is 2.5 μm besides the initial position of the domain wall, inside the domain with brighter contrast. A constant magnetic field of 1.1 mT was applied in the direction favoring expansion of the dark domain. The position of the domain wall along the horizontal direction in the image was determined from PEEM images acquired after individual laser pulses without moving the sample. The scale is defined such that zero corresponds to the left end of the image, while 20 μm refers to the opposite, right side of the image. After each laser pulse, the domain wall moved a bit to the right to expand the dark domain. The solid data points in Fig. 3 show the position of the domain wall after each single laser pulse, measured between successive images. The red continuous line depicts the intensity profile of the laser pulse. It was determined as the cubic root of a Gaussian fit to a line profile along the blue line of a PEEM image of the laser-emitted three-photon photoemission taken directly before the experiment [30].

Starting with pulse number 2, the domain-wall displacement per pulse is around 0.5 μm for 10 pulses, while the domain wall moves about in the center of the laser pulse. Afterwards, when the domain wall reaches the right end of the laser pulse, much higher displacements above 1 μm per pulse are observed. When the domain wall reaches the end of the laser spot, the displacement per pulse eventually reduces. The domain wall thus always moves in the direction of the external magnetic field, but travels more easily in the negative intensity gradient of the laser spot, i.e., when moving

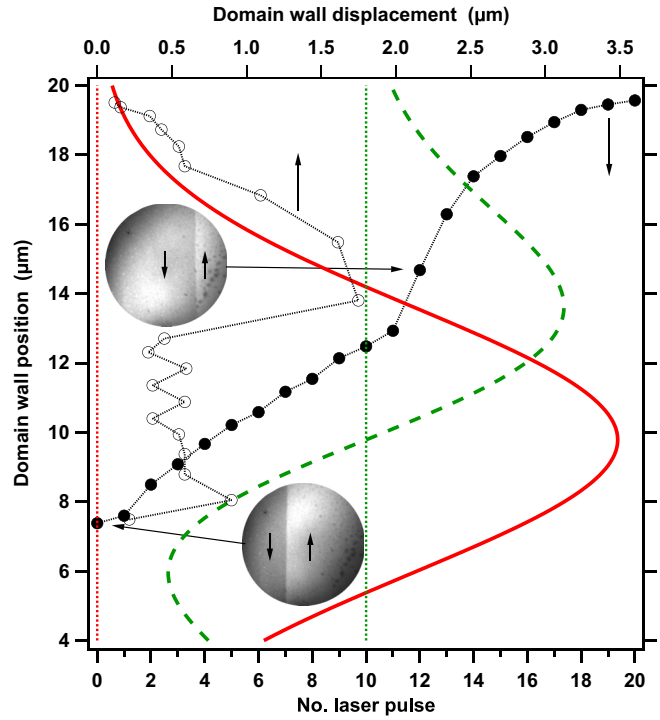

FIG. 3. Solid data points: Position of domain wall after application of individual laser pulses (bottom axis) under 1.1 mT constant magnetic field. Open data points: Distance moved by the domain wall (top axis) at each of the laser pulses, plotted vs the position of the domain wall on the left axis. The two insets show the start image and the image after the 12th laser pulse, taken with positive helicity. Arrows in the insets indicate the local magnetization direction. The external field is pointing downwards in the images. The domain-wall position is measured from left to right along the horizontal direction in the image. Red continuous line: Intensity profile of the laser pulse along the same line. Green dashed line: Derivative of the red curve, showing the intensity gradient. The vertical red and green dotted lines are the respective zero lines. The domain wall travels larger distances upon laser pulse excitation when the motion is away from the center of the laser spot and the gradient of the intensity is high.

towards the colder side of the sample. This is seen most clearly from a plot of the distance moved by the domain wall at each laser pulse as a function of the domain position, presented in Fig. 3 by open symbols. The place where the highest domain-wall displacements around pulse number 12 are observed corresponds to the maximum of the negative gradient of the laser pulse intensity, represented in Fig. 3 by the dashed green line. Although in this experiment the domain wall even at the start was not fully at the positive maximum of the laser intensity gradient, where one expects the maximum laser-pulse-induced force in the direction against the external field, this experiment still gives a rough estimate for the size of the laser-induced steering effect, which is of the same order as the external field, i.e., a few mT.

The motion of domain walls after excitation by laser pulses observed here is similar to the stochastic domain-wall motion observed in Co/Cu/Ni trilayers [11], except that now the domain-wall motion always occurs in one direction, guided by a gradient in the laser pulse and/or the external magnetic field.

The laser-induced domain-wall motion had been explained by a thermal motion of the domain wall after depinning by the laser pulse, for example by thermal excitation during the transient rise of sample temperature or by transient spin currents acting on the domain wall via spin torque [11]. We assume that in the present experiment, the laser pulse also depins the domain wall, which then moves in the predetermined direction to the next pinning site deep enough to pin the wall. Assuming further a constant density of pinning sites with a uniform statistical distribution of pinning strength, a larger displacement of the wall requires a larger force on the domain wall to keep it moving for a longer distance.

In addition to the depinning and stochastic thermal domain-wall motion observed previously [11], here a force pushing the domain wall in a defined direction, away from the hotter to colder areas, has been identified experimentally. We first discuss spin-polarized charge currents as a possible source for this directed domain-wall motion, which due to spin transfer torque could exert a force on a magnetic domain wall [32]. One possibility is that the laser excitation of the sample may lead to superdiffusive currents, which in a ferromagnet become spin polarized [33]. However, lifetimes of such superdiffusive spin currents are expected to be rather short, typically below 1 ps [33]. Even for a very fast domain-wall motion of around 1500 m/s [34], this would lead to a maximum displacement of a domain wall of only around 1.5 nm per laser pulse, probably smaller than the domain-wall width. Considering that the domain wall after ultrafast depinning needs to be pushed away from the previous pinning position into the direction defined by the flux gradient of the laser beam requires a force that lasts of the order of at least several tens of picoseconds. Note that these general timing considerations are independent of whether the sample is ferro- or ferrimagnetic. Also, for the following discussion, the ferrimagnetism of the sample used in the experiment does not play a role. While we cannot exclude a mechanism based on ferrimagnetic order, for example the interaction of polarized magnons existing in antiferromagnetically aligned sublattices with the domain wall [35,36], we believe that at the experimental base temperature far below the compensation temperature, the ferrimagnetic alignment between Gd and Fe moments is of minor importance. Further theoretical work might help to elucidate this point.

Electronic spin currents of longer duration could result from the spin-dependent Seebeck effect [25,26]. Their presence is linked to the lateral thermal gradient on the sample after the laser pulse, which lasts much longer than the electronic excitation. To estimate the size of such spin currents, we simulated the heat flow within the sample by a one-dimensional two-temperature model to investigate the ultrafast laser-material interaction in the z direction, perpendicular to the surface plane [30]. In this model, it is assumed that the laser pulse is absorbed within a few femtoseconds by the conduction electrons of the material. The laser energy is then swiftly thermalized in the conduction band by diffusing hot electrons, before these hot electrons transfer their energy through electron-phonon coupling to the crystal lattice. This leads to an increase of the lattice temperature in a few picoseconds [37]. Lateral heat flow is neglected, which is reasonable since the thickness of the film is much smaller than the lateral

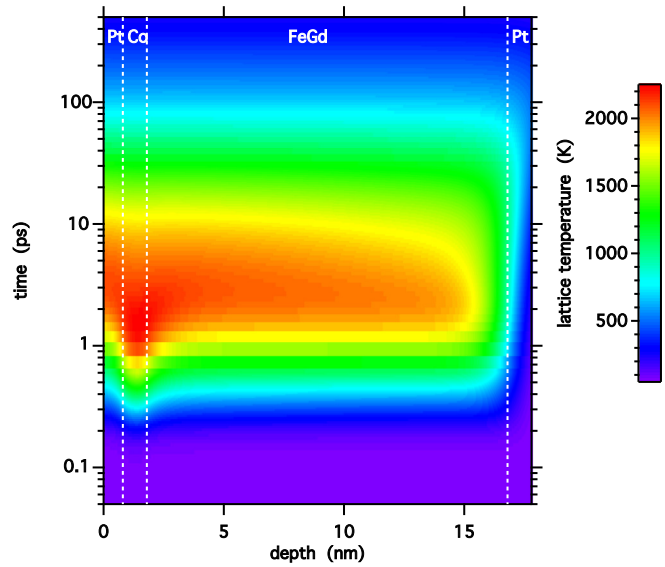

FIG. 4. Time dependence of simulated lattice temperature profile along the film depth, for the maximum fluence of 25 mJ/cm^2 at the center of the laser spot. Dashed vertical lines mark the positions of the interfaces between the different layers.

distances of interest here. In the lateral direction, the laser profile is simply taken as the Gaussian fitted to a PEEM image of the laser pulse, as described before in connection with Fig. 3.

Of interest for the domain-wall displacements is the long-lived lateral temperature gradient resulting from the laterally inhomogeneous exposure to the laser beam, and not the vertical temperature gradient resulting from the excitation of the sample and the heat flow in the vertical direction. The sample cools down by heat flow to the substrate, which serves as a heat sink. Its temperature at the bottom is held constant at 50 K in the simulation.

We find that the maximum lattice temperature calculated for the center of the laser pulse is reached in the Co layer at about 1.4 ps after the pulse with $T_l^{\max} \approx 2200$ K. At that time, the maximum lateral temperature gradient is $\nabla T_x^{\max} = 330 \times 10^6$ K/m in the Co layer and 275×10^6 K/m at 10 nm depth, inside the FeGd layer. After 10 ps, the highest temperature gradient is about 265×10^6 K/m, whereafter it decays with about the same time constant as the lattice temperature, namely, 32 ps. Note that the latter value depends on exactly how the heat flow through the Si substrate is modeled [30], and could also be higher. Figure 4 shows the result for the lattice temperature at the very center of the laser spot across the depth of the film as a function of time after the laser pulse. At the beginning, the highest temperatures are found in the Co layer, while later the temperature across the thickness of the film becomes more uniform. After 100 ps, the multilayer temperature has dropped to about 400 K, and after 1 ns, to about 175 K.

We estimate the maximum spin current J_S generated by these temperature gradients ∇T from

$$J_S = \frac{\sigma_\uparrow S_\uparrow - \sigma_\downarrow S_\downarrow}{\sigma_\uparrow + \sigma_\downarrow} \cdot \nabla T \cdot \sigma, \tag{1}$$

where $\sigma_\uparrow$ and $\sigma_\downarrow$ are the spin-dependent electric conductivities, $\sigma = \sigma_\uparrow + \sigma_\downarrow$ is the spin-independent conductivity, and $S_\uparrow$ and $S_\downarrow$ are the spin-dependent Seebeck coefficients [26]. Since the highest temperatures occur at the Pt/Co interface, we use the parameters for this interface as reported by Choi *et al.* [38], namely, $\sigma = 2.7 \times 10^6\ \Omega^{-1}\,\mathrm{m}^{-1}$ and $\frac{\sigma_\uparrow S_\uparrow - \sigma_\downarrow S_\downarrow}{\sigma_\uparrow + \sigma_\downarrow} \approx 5\ \mu\mathrm{V\,K}^{-1}$. This gives an initial maximum estimated spin current density at the Co layer of $J_S^{\max}$ at 1.4 ps of $\approx 4.5 \times 10^9\ \mathrm{A/m}^2$, which is then gradually dropping. The maximum current density in the FeGd layer is somewhat lower due to the lower temperature gradient. This current density estimated from the model, even shortly after the laser pulse, is at least two orders of magnitude less than the reported spin current density needed for moving domain walls in metallic films, which is in between 10^{11} and $10^{12}\ \mathrm{A/m}^2$ [39–42]. Electronic spin currents generated by the spin-dependent Seebeck effect are thus unlikely to be the source of the observed directed domain-wall motion. While it is the electron temperature that is relevant for the spin-dependent Seebeck effect, it is significantly higher than the lattice temperature only before thermalization of the electronic excitation with the lattice, which occurs in the order of a few-hundred femtoseconds. This is clearly much shorter than needed for any measurable domain-wall motion.

The simulations show that the film transiently demagnetizes in a certain area around the center of the laser spot, where the lattice temperature exceeds the Curie temperature of $Fe_{75}Gd_{25}$ of about 600 K [10]. This demagnetization probably provides the thermal depinning of the domain wall discussed before. Note that it cannot explain the domain-wall motion to the lower-intensity side of the laser spot, since after demagnetization around a domain wall the demagnetized area represents the boundary between the two domains which upon remagnetization is then expected to be at the place of latest remagnetization, i.e., at the center of the laser spot. Considering also the connection of the domain wall to the two remaining ends outside the laser spot, without an additional mechanism pushing it to the colder side of the laser spot, the domain wall would most likely assume its original position since the domain walls observed in this material are always very straight.

This leaves magnonic spin currents resulting from the spin-Seebeck-effect-induced diffusion of magnons from the hotter region with higher magnon density to the cooler region as a possible mechanism for the directed domain-wall motion. However, magnons passing through the domain wall would push it back, towards the hotter side of the sample. The same holds for the entropic force on the domain wall in a temperature gradient [15,16]. Since the opposite, i.e., a motion towards the colder side, is observed, the contribution of magnons reflected at the domain walls, which exerts a force on the wall in the direction towards the colder side [16,18,19], needs to dominate. Reflection at the domain wall occurs if the wavelength of the magnon is large compared to the domain-wall width [16,23]. Theoretical calculations have indeed shown that the average magnon propagation length is mainly related to low-frequency magnons [16]. These are reflected at the domain wall, thereby pushing it to the colder side. A dominating contribution from magnon diffusion due to the temperature gradient can thus explain the observed directed domain-wall motion. We have to note, though, that in Ref. [16] the entropic force was calculated to be stronger than the force from magnonic spin currents from the spin Seebeck effect, in contrast to our observations on the Co/FeGd bilayer.

If a domain wall is more strongly pinned, such as the left domain wall of Fig. 1 at 15 μm x position, the laser-induced domain-wall motion is suppressed. In this case, a higher laser fluence or an excitation closer to the responsible pinning center would probably be necessary to depin the domain wall at that particular position.

IV. CONCLUSION

In conclusion, we observed a directed magnetic domain-wall motion in $Co/Fe_{75}Gd_{25}$ in the intensity gradient of 100 fs infrared laser pulses, in which the domain wall moves away from the center of the laser beam, i.e., towards the direction of lower sample temperature, after the laser pulse. Depending on the position of the domain wall in the gradient of the laser pulse, domain-wall motions of close to a micron could be achieved. An external field of 1.1 mT is sufficient to dominate the direction of the domain-wall motion over the laser-induced force. This gives a quantitative estimate for the upper bound of the laser-induced directionality effect: It has to be smaller than an effective field of 1.1 mT. Quantitative estimates of the temporal duration and the strength of electronic spin currents excited by the laser pulse, either as diffusive currents or by the spin-dependent Seebeck effect in the temperature gradient, are too small to explain the experimental observations. We suggest laser-induced depinning by thermal demagnetization of domain walls and successive recoil of magnons diffusing in the thermal gradient of the laser-heated spot at the domain walls instead as a likely mechanism of the directed laser-induced domain-wall motion. An entropy-driven force, which would act on the domain wall in the opposite direction, has to be smaller than the magnon-related force in our samples. It would be interesting to see how important the laser-induced depinning of domain walls is and which effect static temperature gradients of the same size would have.

While the direction of the laser-induced domain-wall motion is possibly material specific, the possibility to move magnetic domain walls in a defined way by a laterally inhomogeneous ultrafast optical excitation should be a more general effect, which we expect to be present also in other materials with a sufficiently low density of pinning sites for domain walls. Employing near-field optics to focus the laser spot on the sample, domain walls could be moved with higher precision and with less sensitivity to defects because of the stronger lateral gradient. The chance to steer domain walls with ultrashort optical pulses is very interesting for writing or processing magnetic information in artificially structured materials. Our experimental finding might trigger further theoretical work to quantitatively describe the underlying mechanism in detail and to predict and optimize the effect in different materials.

ACKNOWLEDGMENTS

Funding by the DFG (Grant No. Ku 1115/11-1 and Project No. A07 of CRC/TRR 227) and the Focus Area Nanoscale of Freie Universität Berlin is gratefully acknowledged. Y.A.S.

thanks the MoHE and the DAAD for financial support through a GERLS scholarship. J.V. acknowledges PHC Procope for a grant (Project No. 28558NE). We thank the HZB for the allocation of synchrotron radiation beam time and U. Atxitia, J. Berakdar, P. Brouwer, U. Nowak, and X. Waintal for fruitful discussions.

[1] S. S. P. Parkin, M. Hayashi, and L. Thomas, Magnetic domain-wall racetrack memory, Science **320**, 190 (2008).

[2] I. M. Miron, G. Gaudin, S. Auffret, B. Rodmacq, A. Schuhl, S. Pizzini, J. Vogel, and P. Gambardella, Current-driven spin torque induced by the Rashba effect in a ferromagnetic metal layer, Nat. Mater. **9**, 230 (2010).

[3] S.-H. Yang, K.-S. Ryu, and S. Parkin, Domain-wall velocities of up to 750 m s^{-1} driven by exchange-coupling torque in synthetic antiferromagnets, Nat. Nanotech. **10**, 221 (2015).

[4] A. Stupakiewicz, K. Szerenos, D. Afanasiev, A. Kirilyuk, and A. V. Kimel, Ultrafast nonthermal photo-magnetic recording in a transparent medium, Nature (London) **542**, 71 (2017).

[5] A. V. Kimel, A. Kirilyuk, P. A. Usachev, R. V. Pisarev, A. M. Balbashov, and T. Rasing, Ultrafast non-thermal control of magnetization by instantaneous photomagnetic pulses, Nature (London) **435**, 655 (2005).

[6] A. J. Ramsay, P. E. Roy, J. A. Haigh, R. M. Otxoa, A. C. Irvine, T. Janda, R. P. Campion, B. L. Gallagher, and J. Wunderlich, Optical Spin-Transfer-Torque-Driven Domain-Wall Motion in a Ferromagnetic Superconductor, Phys. Rev. Lett. **114**, 067202 (2015).

[7] T. A. Ostler, J. Barker, R. F. L. Evans, R. W. Chantrell, U. Atxitia, O. Chubykalo-Fesenko, S. El Moussaoui, L. Le Guyader, E. Mengotti, L. J. Heyderman, F. Nolting, A. Tsukamoto, A. Itoh, D. Afanasiev, B. A. Ivanov, A. M. Kalashnikova, K. Vahaplar, J. Mentink, A. Kirilyuk, T. Rasing, and A. V. Kimel, Ultrafast heating as a sufficient stimulus for magnetization reversal in a ferrimagnet, Nat. Commun. **3**, 666 (2012).

[8] A. R. Khorsand, M. Savoini, A. Kirilyuk, A. V. Kimel, A. Tsukamoto, A. Itoh, and T. Rasing, Role of Magnetic Circular Dichroism in All-Optical Magnetic Recording, Phys. Rev. Lett. **108**, 127205 (2012).

[9] S. Mangin, M. Gottwald, C.-H. Lambert, D. Steil, V. Uhlíř, L. Pang, M. Hehn, S. Alebrand, M. Cinchetti, G. Malinowski, Y. Fainman, M. Aeschlimann, and E. E. Fullerton, Engineered materials for all-optical helicity-dependent magnetic switching, Nat. Mater. **13**, 286 (2014).

[10] L. Le Guyader, S. El Moussaoui, M. Buzzi, M. Savoini, A. Tsukamoto, A. Itoh, A. Kirilyuk, T. Rasing, F. Nolting, and A. V. Kimel, Deterministic character of all-optical magnetization switching in GdFe-based ferrimagnetic alloys, Phys. Rev. B **93**, 134402 (2016).

[11] O. Sandig, Y. A. Shokr, J. Vogel, S. Valencia, F. Kronast, and W. Kuch, Movement of magnetic domain walls induced by single femtosecond laser pulses, Phys. Rev. B **94**, 054414 (2016).

[12] T. Eggebrecht, M. Möller, J. G. Gatzmann, N. Rubiano da Silva, A. Feist, U. Martens, H. Ulrichs, M. Münzenberg, C. Ropers, and S. Schäfer, Light-Induced Metastable Magnetic Texture Uncovered by in Situ Lorentz Microscopy, Phys. Rev. Lett. **118**, 097203 (2017).

[13] T. Janda, P. E. Roy, R. M. Otxoa, Z. Šobáň, A. Ramsay, A. C. Irvine, F. Trojanek, M. Surýnek, R. P. Campion, B. L. Gallagher, P. Němec, T. Jungwirth, and J. Wunderlich, Inertial displacement of a domain wall excited by ultra-short circularly polarized laser pulses, Nat. Commun. **8**, 15226 (2017).

[14] Y. Quessab, R. Medapalli, M. S. El Hadri, M. Hehn, G. Malinowski, E. E. Fullerton, and S. Mangin, Helicity-dependent all-optical domain wall motion in ferromagnetic thin films, Phys. Rev. B **97**, 054419 (2017).

[15] F. Schlickeiser, U. Ritzmann, D. Hinzke, and U. Nowak, Role of Entropy in Domain Wall Motion in Thermal Gradients, Phys. Rev. Lett. **113**, 097201 (2014).

[16] S. Moretti, V. Raposo, E. Martinez, and L. Lopez-Diaz, Domain wall motion by localized temperature gradients, Phys. Rev. B **95**, 064419 (2017).

[17] D. Hinzke and U. Nowak, Domain Wall Motion by the Magnonic Seebeck Effect, Phys. Rev. Lett. **107**, 027205 (2011).

[18] A. Sukhov, L. Chotorlishvili, A. Ernst, X. Zubizarreta, S. Ostanin, I. Mertig, E. K. U. Gross, and J. Berakdar, Swift thermal steering of domain walls in ferromagnetic MnBi stripes, Sci. Rep. **6**, 24411 (2016).

[19] P. Yan, Y. Cao, and J. Sinova, Thermodynamic magnon recoil for domain wall motion, Phys. Rev. B **92**, 100408(R) (2015).

[20] J. Torrejon, G. Malinowski, M. Pelloux, R. Weil, A. Thiaville, J. Curiale, D. Lacour, F. Montaigne, and M. Hehn, Unidirectional Thermal Effects in Current-Induced Domain Wall Motion, Phys. Rev. Lett. **109**, 106601 (2012).

[21] W. Jiang, P. Upadhyaya, Y. Fan, J. Zhao, M. Wang, L.T. Chang, M. Lang, K. L. Wong, M. Lewis, Y. T. Lin, J. Tang, S. Cherepov, X. Zhou, Y. Tserkovnyak, R. N. Schwartz, and K. L. Wang, Direct Imaging of Thermally Driven Domain Wall Motion in Magnetic Insulators, Phys. Rev. Lett. **110**, 177202 (2013).

[22] J.-P. Tetienne, T. Hingant, J.-V. Kim, L. Herrera Diez, J.-P. Adam, K. Garcia, J.-F. Roch, S. Rohart, A. Thiaville, D. Ravelosona, and V. Jacques, Nanoscale imaging and control of domain-wall hopping with a nitrogen-vacancy center microscope, Science **344**, 1366 (2014).

[23] Xi-guang Wang, Guang-hua Guo, Yao-zhuang Nie, Guang-fu Zhang, and Zhi-xiong Li, Domain wall motion induced by the magnonic spin current, Phys. Rev. B **86**, 054445 (2012).

[24] Se Kwon Kim and Y. Tserkovnyak, Landau-Lifshitz theory of thermomagnonic torque, Phys. Rev. B **92**, 020410(R) (2015).

[25] M. Johnson and R. H. Silsbee, Thermodynamic analysis of interfacial transport and of the thermomagnetoelectric system, Phys. Rev. B **35**, 4959 (1987).

[26] A. Slachter, F. L. Bakker, J. P. Adam, and B. J. van Wees, Thermally driven spin injection from a ferromagnet into a non-magnetic metal, Nat. Phys. **6**, 879 (2010).

[27] J. Stöhr, Y. Wu, B. D. Hermsmeier, M. G. Samant, G. R. Harp, S. Koranda, D. Dunham, and B. P. Tonner, Element-specific magnetic microscopy with circularly polarized x-rays, Science **259**, 658 (1993).

[28] W. Kuch, R. Schäfer, P. Fischer, and F. U. Hillebrecht, *Magnetic Microscopy of Layered Structures*, Springer Series in Surface Sciences, Vol. 57 (Springer, Berlin, 2015).

[29] F. Kronast, J. Schlichting, F. Radu, S.K. Mishra, T. Noll, and H.A. Dürr, Spin-resolved photoemission microscopy and magnetic imaging in applied magnetic fields, Surf. Interf. Anal. **42**, 1532 (2010).

[30] See Supplemental Material at http://link.aps.org/supplemental/10.1103/PhysRevB.99.214404, which contains element-resolved magnetic domain images, magneto-optical Kerr effect measurements, element-resolved magnetization loops, domain images showing the motion of the trapped domain wall upon laser pulses, details about the two-temperature-model simulations used to estimate the transient sample temperature, more information on the determination of the laser profile, and includes Refs. [8,43–55].

[31] T. A. Ostler, R. F. L. Evans, R. W. Chantrell, U. Atxitia, O. Chubykalo-Fesenko, I. Radu, R. Abrudan, F. Radu, A. Tsukamoto, A. Itoh, A. Kirilyuk, Th. Rasing, and A. Kimel, Crystallographically amorphous ferrimagnetic alloys: Comparing a localized atomistic spin model with experiments, Phys. Rev. B **84**, 024407 (2011).

[32] T. Taniguchi, J. Sato, and H. Imamura, Theory of spin accumulation and spin-transfer torque in a magnetic domain wall, Phys. Rev. B **79**, 212410 (2009).

[33] M. Battiato, K. Carva, and P. M. Oppeneer, Superdiffusive Spin Transport as a Mechanism of Ultrafast Demagnetization, Phys. Rev. Lett. **105**, 027203 (2010).

[34] E. R. Lewis, D. Petit, L. O'Brien, A. Fernandez-Pacheco, J. Sampaio, A-V. Jausovec, H. T. Zeng, D. E. Read, and R. P. Cowburn, Fast domain wall motion in magnetic comb structures, Nat. Mater. **9**, 980 (2010).

[35] Jin Lan, Weichao Yu, and Jiang Xiao, Antiferromagnetic domain wall as spin wave polarizer and retarder, Nat. Commun. **8**, 178 (2017).

[36] Weichao Yu, Jin Lan, and Jiang Xiao, Polarization-selective spin wave driven domain-wall motion in antiferromagnets, Phys. Rev. B **98**, 144422 (2018).

[37] Jau Tang, Nanoscale heat transfer in a thin aluminum film and femtosecond time-resolved electron diffraction, Appl. Phys. Lett. **92**, 011901 (2008).

[38] Gyung-Min Choi, Byoung-Chul Min, Kyung-Jin Lee, and D. G. Cahill, Spin current generated by thermally driven ultrafast demagnetization, Nat. Commun. **5**, 5334 (2014).

[39] F. J. Albert, J. A. Katine, R. A. Buhrman, and D. C. Ralph, Spin-polarized current switching of a Co thin film nanomagnet, Appl. Phys. Lett. **77**, 3809 (2000).

[40] M. Tsoi, A. G. M. Jansen, J. Bass, W.-C. Chiang, M. Seck, V. Tsoi, and P. Wyder, Excitation of a Magnetic Multilayer by an Electric Current, Phys. Rev. Lett. **80**, 4281 (1998).

[41] L. Berger, Emission of spin waves by a magnetic multilayer traversed by a current, Phys. Rev. B **54**, 9353 (1996).

[42] M. Yamanouchi, D. Chiba, F. Matsukura, and H. Ohno, Current-induced domain-wall switching in a ferromagnetic semiconductor structure, Nature (London) **428**, 539 (2004).

[43] Y. Zhang and J. K. Chen, Ultrafast melting and resolidification of gold particle irradiated by pico- to femtosecond lasers, J. Appl. Phys. **104**, 054910 (2008).

[44] S. I. Anisimov, B. L. Kapeliovich, and T. L. Perel'man, Electron emission from metal surfaces exposed to ultrashort laser pulses, Zh. Eksp. Teor. Fiz. **66**, 776 (1974) [Sov. Phys.-JETP **39**, 375 (1974)].

[45] K. Ohta and H. Ishida, Matrix formalism for calculation of the light beam intensity in stratified multilayered films, and its use in the analysis of emission spectra, Appl. Opt. **29**, 2466 (1990).

[46] A. P. Caffrey, P. E. Hopkins, J. M. Klopf, and P. M. Norris, Thin film non-noble transition metal thermophysical properties, Microscale Thermophys. Eng. **9**, 365 (2005).

[47] W. S. M. Werner, K. Glantschnig, and C. Ambrosch-Draxl, Optical constants and inelastic electron-scattering data for 17 elemental metals, J. Phys. Chem. Ref. Data **38**, 1013 (2009).

[48] P. B. Johnson and R. W. Christy, Optical constants of transition metals: Ti, V, Cr, Mn, Fe, Co, Ni, and Pd, Phys. Rev. B **9**, 5056 (1974).

[49] K. Vahaplar, A. M. Kalashnikova, A. V. Kimel, D. Hinzke, U. Nowak, R. Chantrell, A. Tsukamoto, A. Itoh, A. Kirilyuk, and Th. Rasing, Ultrafast Path for Optical Magnetization Reversal via a Strongly Nonequilibrium State, Phys. Rev. Lett. **103**, 117201 (2009).

[50] A. M. Chen, Y. F. Jiang, L. Z. Sui, H. Liu, M. X. Jin, and D. J. Ding, Thermal analysis of double-layer metal films during femtosecond laser heating, J. Opt. **13**, 055503 (2011).

[51] A. S. Okhotin, A. S. Pushkarskii, and V. V. Gorbachev, *Thermophysical Properties of Semiconductors* (Atom Publ. House, Moscow, 1972).

[52] C. J. Glassbrenner and G. A. Slack, Thermal conductivity of silicon and germanium from 3°K to the melting point, Phys. Rev. **134**, A1058 (1964).

[53] M. Colina, C. Molpeceres, M. Morales, F. Allens-Perkins, G. Guadaño, and J. L. Ocaña, Laser ablation modelling of aluminium, silver and crystalline silicon for applications in photovoltaic technologies, Surface Engineering **27**, 414 (2011).

[54] J. Pudell, A. A. Maznev, M. Herzog, M. Kronseder, C. H. Back, G. Malinowski, A. von Reppert, and M. Bargheer, Layer specific observation of slow thermal equilibration in ultrathin metallic nanostructures by femtosecond x-ray diffraction, Nat. Commun. **9**, 3335 (2018).

[55] Y. Shokr, Interaction Mechanisms and Magnetization Dynamics in Ultrathin Antiferromagnetic Films and their Correlation with Structure and Morphology, Ph.D. thesis, Freie Universität Berlin, Berlin (2016).